CONF-831203--72

CONF-831203--72

DE84 004687

DIAGNOSTIC TECHNIQUES FOR MEASURING TEMPERATURE TRANSIENTS AND STRESS TRANSIENTS IN THE FIRST WALL OF AN ICF REACTOR

N. T. Melamed and L. H. Taylor
Westinghouse R&D Center
Pittsburgh, Pennsylvania 15235

ABSTRACT

The primary challenge in the design of an Inertial Confinement Fusion (ICF) power reactor is to make the first wall survive the frequent explosions of the pellets. Westinghouse has proposed a dry wall design consisting of steel tubes coated with tantalum. This report describes the design of a test chamber and two diagnostic procedures for experimentally determining the reliability of the Westinghouse design. The test chamber simulates the x-ray and ion pulse irradiation of the wall due to a pellet explosion. The diagnostics consist of remote temperature sensing and surface deformation measurements. The chamber and diagnostics can also be used to test other first-wall designs.

1. INTRODUCTION AND SUMMARY

One of the basic problems in fusion reactors is the design of the first wall of the reactor chamber. This wall must withstand the repeated onslaught of the combined effects of radiation and ions produced by the pellet explosions. Recently Westinghouse proposed a dry first wall comprised of 0.18 cm wall steel tubes coated with approximately 0.1 cm of tantalum.[16] The tantalum coating resists the effects of the radiation and ion bombardment, while liquid lithium metal, flowing within the tubes, carries away the heat produced.

Any wall protection scheme must of course last for years in the very hostile environment of the ICF reactor. Although many analytical studies have been performed on these schemes, many uncertainties remain which can only be resolved by experimental measurements. These uncertainities include, but are not limited to, the effects of:

- Very short but intense temperature spikes
- Sputtering
- Chemical reactions
- Fatigue

Another feature of interest in laser-driven ICF reactors is an examination of the effects resulting from radiation trapping and blast waves generated in the 0.1 Torr of gas present in these reactors. The latter effects will also occur in light ion-driven reactors which require a high pressure gas for their operation, but will be absent in heavy ion-driven ractors which require gas pressures below 10^{-5} Torr.

To determine the validity of the dry wall design as well as other wall protection schemes, a simulation facility must therefore be built to investigate the net effect of these complicated processes.[22] To facilitate the eventual construction of such a facility, a scoping study has been undertaken and is reported herein. The next section outlines the general system considerations for this facility, and is followed by sections on the pulse sources and experimental diagnostics.

More specifically, the next section includes a general schematic of the overall system which shows the spatial relationships of the pulse energy sources, the first wall sample, and the diagnostic equipment. The section also includes an analysis which shows that the beams from the pulse sources must have a minimum radius to produce a good simulation of expected ICF reactor conditions. To simulate reactor conditions during the x-ray and ion pulses the minimum beam radius is 0.55 cm, whereas to simulate reactor conditions between pellet explosions, at 10 explosions per second, the minimum beam radius is 2.0 cm.

In examining sources to simulate the x-ray pulse, three types of sources were considered for the production of irradiances of 10 MW/cm^2 in pulses lasting for tens of nanoseconds. These source types were a) characteristic, b) bremsstrahlung, and c) transition. Bremsstrahlung radiation is relatively strong at short wavelengths while transition radiation is strong at long wavelengths. To generate the high irradiance in a short pulse, special electron guns would be required. Alternative sources which could satisfy these requirements are commercially available chemical or carbon dioxide lasers.

To simulate the ion pulse, two types of ion beam sources were considered for the production of irradiance of 50 kW/cm^2 in pulses lasting for tens of microseconds. Although, in principle, either field ionization or large area spark sources could be used, the spark source is probably the better source. In either case, significant development would be needed to achieve the high ion current (4 A/cm^2) and beam radius with the proper ion species.

To simulate the ICF reactor environment, the x-ray beam will strike the first wall sample a few microseconds before the ion beam. These impinging beams will raise the temperature of the sample and produce stresses within it. To fully understand the effects on the sample, the temperature and stress must be measured as a function of time and of location in the sample.

The temperature is measured with two-color radiation pyrometry. By focusing an image of the sample surface onto a fast vidicon detector, a 10 degree change at 3000°K can be determined with a temporal resolution of one microsecond. The stresses are inferred[23,24] from holographic interferometric measurements of the surface deformations. Pulsed ruby lasers allow temporal resolutions of 20 nsec. Since both techniques involve images of the sample surface, the desired spatial resolution is readily available.

2. SYSTEM CONSIDERATIONS

2.1 Sample Size

In a well designed ICF spherical reactor chamber the x-ray and ion fluxes will be normal to the wall. Lateral temperature gradients along the wall surface should therefore not be significant and must be avoided in any simulation facility. On the other hand, temperature gradients normal to the surface will be very large and will have significant time dependencies. This behavior must not be significantly modified by the design of the simulation facility.

In the simulator a circular beam of radius a and irradiance H will impinge on a small sample of the first wall. The lateral heat conduction in the sample, relative to the normal heat conduction into the sample, will be a function of the beam radius and sample size. Consider first the case where the sample is much larger than the beam. The heat flow in the lateral direction is difficult to calculate and is beyond the intent of this study. However, the ratio of the lateral heat flow to the normal heat flow is, to zero order, simply the ratio of the areas through which the heat flows:

$$f = 2\pi a \ell / \pi^2$$

$$= 2\ell/a \qquad (1)$$

where ℓ is the effective depth of penetration of the heat flow.

The depth ℓ at the end of the heating pulse can be estimated from the analytical solution for the sudden heating of a semi-infinite solid:[1]

$$\ell \approx 0.6 \sqrt{\alpha\tau} \qquad (2)$$

In this expression the right hand side is the analytical solution for the depth at which the temperature is 1/2 the value at the surface. In this expression τ is the temporal width of the heating pulse and α is the thermal diffusivity of the coating:

$$\alpha = k/\rho C \quad cm^2/sec \tag{3}$$

where k, ρ, and C are the thermal conductivity, mass density, and specific heat, respectivity. For tantalum

$$\alpha = 0.2174 \quad cm^2/sec \tag{4}$$

The X-ray pulse nominally lasts for tens of nanoseconds. For a 100 nsec pulse the above expressions indicate that the effective depth at the end of the pulse will be 0.9 μm whereas the effective depth will be 28 μm for a 100 μsec pulse. For a 1% loss factor (Equation 1) the beam radius must be 0.55 cm and the sample size must be larger than this, i.e., it must have more than 0.95 cm^2 of area.

These requirements are sufficient if the main concern is intrapulse behavior. However, the relaxation behavior of the wall between pulses is also of interest but will require a much larger sample. For a 10 pps reactor the time between pulses is 100 msec. However, in this case it is not the time which is important but rather the coating thickness and we can simply set the penetration depth to that thickness. Thus, for a 1.0 mm thick coating and a 10% loss factor the beam radius must be 2 cm and the area of the sample must be larger than 13 cm^2. This sample size should be no problem to fabricate, but the 2 cm radius beam can be a severe limitation on the pulse sources since the energies required from the sources scale as the beam radius squared.

An alternative to large sample sizes and beam radii is to use a very small sample in which the entire surface is irradiated with the incident beam. In this case the lateral flow is reduced since it occurs

by the much less efficient radiation of energy from the sample sides. This approach has many advantages since the thermal behavior of the wall sample can be viewed directly along the side, and the energy requirements on the beam are much less. The main disadvantages are the difficulties of handling small samples, and correlating the thermal behavior of the small sample to the expected behavior of the large reactor wall.

2.2 System Configuration

The general system configuration is shown schematically in Fig. 1. A pulsed X-ray source of the proper energy and time duration is fired first into a relatively large cylinder which contains a controlled gas environment. The beam travels through the gas and strikes the sample at the opposite end. At the appropriate time a pulsed ion source of the proper energy and time duration is fired into the cylinder and its beam also strikes the sample. The firing of the two beams is controlled so as to simulate the arrival of the x-ray and ion pulses at the first wall of an ICF reactor.

The controlled gas environment may be a near vacuum (10^{-5} Torr) to simulate the heavy ion reactor, may vary up to 10^{-1} Torr to simulate the laser reactor, or up to 100 Torr to simulate the light ion reactor. The gas constituents may also be varied to simulate the actual environment expected in a reactor. The gas handling apparatus for controlling this environment is not shown in Fig. 1.

For gas pressures above 10^{-2} Torr pressure waves will be formed in the gas from the energy deposited by the x-ray and ion beams. The effect of these shock waves on the sample may be important. To simulate these shock waves, and the accompanying gas heating, the radius of the muffler should only be slightly larger than the radii of the beams. The muffler, a tube containing numerous holes, damps the shock waves traveling toward the tube walls. By preventing these waves from striking the sample after being reflected off the wall, the simulation

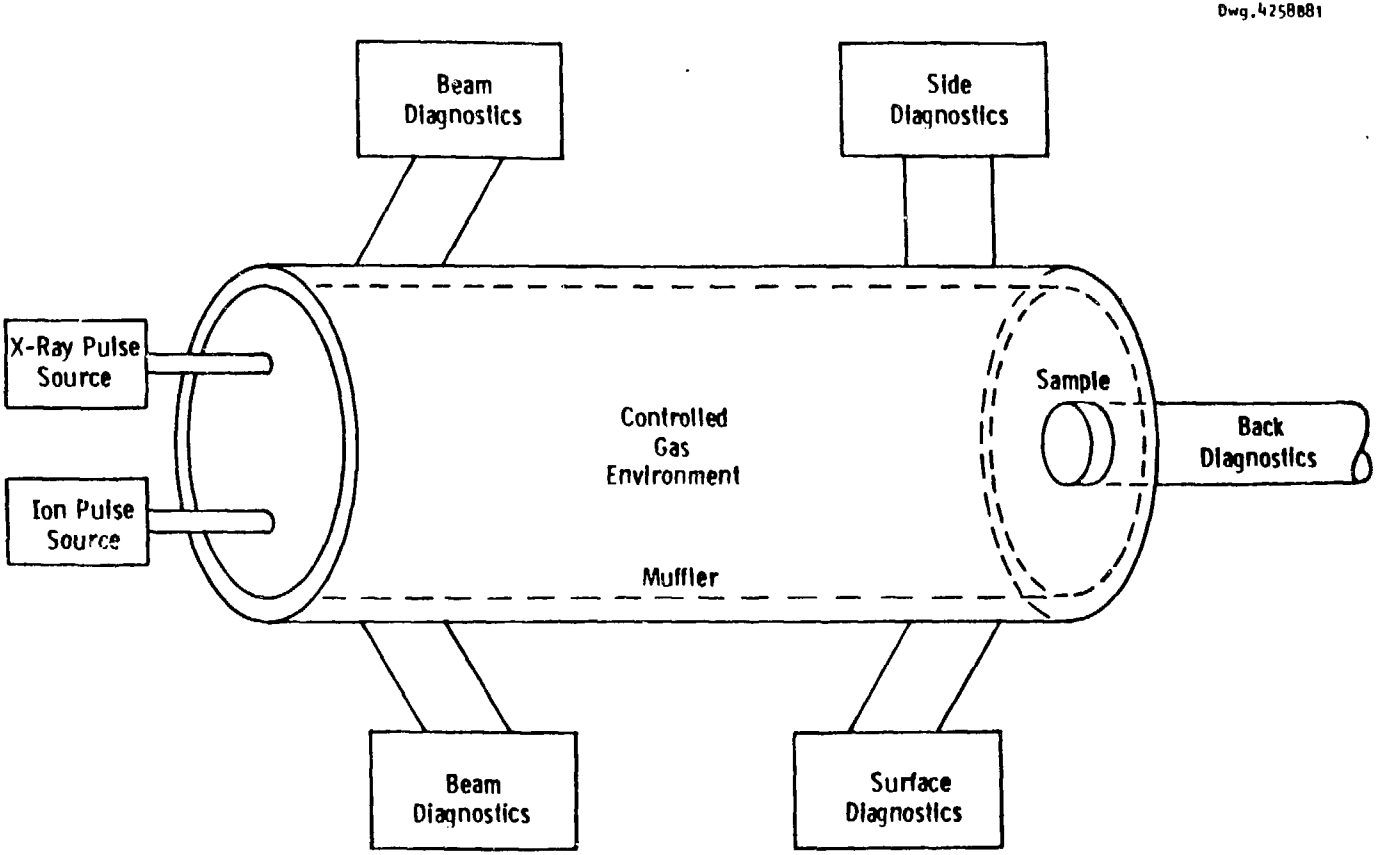

Fig. 1 - General system configuration for simulation facility.

of a large reactor cavity which would not have these walls is not degraded. Acoustical absorbing materials may also be placed between the muffler and the outer wall.

The length of the tube is unimportant for pressures below 10^{-2} Torr. However, for higher pressures the tube length becomes important and in reality should be the same as the radius of the ICF reactor cavity being simulated. Although many gas pressure effects scale as the product of pressure and distance, thereby allowing the tube length to be shortened in exchange for a higher gas pressure, such scaling is not universally valid. In fact, many nonlinear effects such as radiation trapping may be significant.[2-4]

Since sputtering of the sample may be important, it also would be desirable to heat the entire tube to a temperature higher than the steady-state temperature of the sample. This would allow any sputtered material to recondense onto the sample rather than on to the tube walls.

Another feature which should be incorporated into the simulator is the ability to turn the sample so the beams may strike its surface at an angle. This capability would allow the simulation of circular reactor cavities as well as of spherical cavities.

Also sketched in Fig. 1 are apparatuses for monitoring the performance of the beams and for studying the behavior of the sample. Not shown is an apparatus for monitoring the state of the controlled gas environment. The apparatus for monitoring the beams and gas are rather standard and will not be discussed further. However, the pulsed energy sources and sample diagnostic methods are not so conventional and will be discussed in the next two sections.

3. PULSED POWER SOURCES

3.1 X-Ray Sources

The x-ray spectrum from the pellet explosion can be divided into two parts: hard x-rays (10 keV or above) and soft x-rays (1 keV or lower). The hard x-rays penetrate deeply into the chamber wall and heat slightly a large volume of the wall. Conversely, the soft x-rays have little penetration and generate a large temperature spike at the surface of the wall. Although the hard x-rays can be safely neglected, it is important to simulate the soft x-ray pulse, which only lasts for tens of nanoseconds and produces an irradiance of 10 MW/cm^2 or higher.

One source of x-rays is the synchrotron radiation from an electron accelerator which constrains the electrons in a curved path. This radiation is tunable with a broad and intense energy spectrum. However, it is only generated in large, cumbersome devices operating at high energies and cannot be considered seriously for the ICF simulator facility.[5,6]

The simplest and most promising x-ray source for the simulator facility is one which uses the electron impact on metals to produce the x-rays. The electrons are obtained from a cathode by either field emission and/or thermionic emission. The electrons are then accelerated and focused onto the target by electromagnetic means which can be easily pulsed. The basic design of these compact x-ray tubes has been described by Barrie.[7]

When an electron enters a metal target, three types of radiation are produced:

- Characteristic
- Bremsstrahlung
- Transition

The x-ray energies of the characteristic radiation spectrum are quite narrow and intense since they arise from the electronic transitions of the atoms in the target. Since the spectrum of the x-ray source should fairly closely match the expected ICF spectrum, it is therefore important that the electron target material be, as much as is possible, the same material as the ICF pellet, e.g., tantalum.

Bremsstrahlung radiation is a volume effect resulting from multiple collision processes as the electrons lose their energy and are finally brought to rest. This is the most common source of x-ray radiation and is very promising for the simulator facility. Hughes, Heumier, and Griffin have even published the Bremsstrahlung and characteristic radiation spectrum of tantalum under bombardment with 3 keV electrons.[8] To obtain very soft x-rays where absorption by the target may be a serious problem the solid metal target may be replaced by a metallic vapor obtained by evaporating a slug of solid metal.[9]

In contrast to bremsstrahlung radiation, transition radiation is a suface effect which occurs when a charged particle crosses the boundary between two media with different dielectric constants. Since it is a surface effect, the radiation from multiple boundaries in a periodic structure can be made to add coherently in certain directions. As a result very intense and directional x-rays are obtained which may be two orders of magnitude higher than those obtained from a synchrotron source.[10]

Bremsstrahlung, in general, is a relatively strong source of radiation at the short wavelengths whereas transition radiation is strong at the long wavelengths. The two forms of radiation therefore complement each other. This complementary nature is seen in the spectra from tantalum, where the bremsstrahlung radiation decreases from 100 Å to 1000 Å beyond which it is very weak. By contrast, the transition radiation decreases from 500 Å to 5000 Å beyond which it becomes very weak.[8]

The main limitation of these x-ray sources is the electron gun which, instead of generating x-rays, can also be used to heat the wall sample directly.[21] Because of the small penetration depth of soft x-rays, heating by electrons is quite a good approach. The two major problems with the electron simulation technique is that direct electron heating cannot simulate the characteristic radiation, which may or may not be significant, and that the generation of shock waves in gases will be quite different for electron beams than for x-ray beams.

Although commercial electron guns satisfying the performance specifications needed for the simulation facility do not exist, there are some that come close and may be modified for use in the facility. For example, a transverse electron gun design developed at the Colorado State University can give 80 kW in a 2 μsec pulse of 1-10 kV electrons.[11] At Westinghouse we have a wire ion plasma (WIP) 54 kW 150 kV electron gun capable of operating at 10 kHz with pulse widths of 200-600 nsec.

It is clear that some development work remains to be completed before an electron gun with the proper specifications can be used either for directly heating the sample or for generating the desired x-ray beam. A more reasonable approach, at least in the short term, may be to use laser irradiation to heat the sample. Commercially available lasers already exist which are satisfactory, such as the hydrogen fluoride or deuterium fluoride chemical laser (50-200 nsec pulses, 2-600 mJ/pulse, 0.1-2 cm beam radius) and the carbon dioxide laser (50 nsec - 75 μsec, 0.03-75 J/pulse, 0.2-5 cm beam radius).[12]

In addition to the problem of the high reflectivity of metallic surfaces, the main problem with using lasers is in the fact that the interaction of the laser radiation with the sample surface is complicated and undoubtedly does not simulate too closely the x-ray radiation effects.[13,14] On the other hand, if the effects are primarily caused by simple heating and heat flow, laser irradiation should be quite satisfactory. In any event, lasers are presently the best candidate for the "x-ray pulsed source."

3.2 Ion Sources

The arrival of the ion pulse at the ICF reactor wall occurs many microseconds after the x-ray pulse, and lasts for tens of microseconds with an irradiance of 50 kW/cm^2 or higher. Although the ion pulse has much more energy, its significantly lower power reduces the heating effects in the chamber wall. As with the x-ray pulse, the ions have relatively little penetration into the surface, indicating that the thermal effect of an ion pulse can be closely simulated by a surface heating pulse such as can be obtained with a laser beam. However, the long term effects of sputtering and ion contamination of the sample can only be studied with a true ion beam comprised of ions that closely approximate the ions expected from an ICF pellet explosion.

There are many ionization techniques and concepts used to generate ion beams. Unfortunately, the high ion current (> 4 A/cm^2) required for the ICF ion pulse simulator limits the possibilities to only two:

- o Field Ionization Source
- o Spark Source

Both sources, however, produce small radius beams.

The field ionization source obtains its ions by ionizing atoms near a sharp point where the electric field is extremely high, whereas the spark source generates its ions in a spark discharge, usually between two electrodes fabricated of the atoms from which the desired ions are to be obtained. The very nature of these processes restricts the field ionization source to relatively low ion currents (< 10^{-8}A). On the other hand, large area spark sources (5-7 cm^2) have produced 50-200A of light ions in lasting for pulses.[15] It thus appears that an improved spark source would be capable of producing the desired ion beam.

4. EXPERIMENTAL DIAGNOSTICS

4.1 Measurements Desired

The effects of a thermonuclear fusion lead to the production of soft x-radiation and rapidly travelling ions. The x-ray pulse produced by a single pellet is expected to last some tens of nanoseconds, and, for a 10 meter radius chamber, will reach the wall about 35 nsec after the implosion. The ion pulse will arrive a few μsecs later, and is expected to last many microseconds. The primary affect of the two pulses is to cause very rapid increase in the surface temperature of the wall, with the maximum temperature, produced by the soft x-rays, reaching as high as perhaps 3000°K, close to the melting point of tantalum. Such a rapid rise in temperature will produce a momentary deformation of the surface and an acoustic wave that will propagate both along the surface and into the wall. These effects, in turn, will produce stresses in the chamber wall that will affect the wall integrity.

In studying the immediate effects of a simulated pellet explosion, a primary measurement must be the temporal and spacial dependence of the temperature. Secondary desired measurements are those that record the surface deformation, and the propagation of the acoustic wave produced.

The measurements ideally should be taken with a time resolution equal to or less than the fastest significant event, i.e., $t \leq 10^{-6}$ sec, by methods that do not perturb the phenomena to be measured, and in an environment that conservatively can be labeled as hostile. Although mathematical modelling of the effects of a pellet explosion show that the temperature rise and decay is confined to the Ta coating,[16] clearly some effects will be felt by the steel substrate. Thus, measurements

across the entire cross section of the wall are desired, over a time period of perhaps milliseconds, considerably longer than merely the duration of the pulses. The ultimate aim is to acquire sufficient data to permit calculations of the stresses produced. Long term effects on the vessel wall, such as bulk damage, effects on the Ta to steel adhesion, etc., that result from repeated exposure to pellet fusions can be studied by more conventional methods.

In the sections that follow, we describe possible measurement techniques for obtaining the desired information. Following this, we discuss the facilities that are available for these measurements, and the possible difficulties to be encountered.

4.2 Temperature Measurement

GENERAL DESCRIPTION

As mentioned above, the temporal and spacial dependence of the wall temperature following a pellet explosion constitutes a basic measurement. The two most common methods of temperature measurement are use of a thermal probe, such as a thermocouple, and optical pyrometry. Thermocouples are inherently slow, and have the further disadvantage of having to be attached to the surface. The attachment perturbs the surface and may distort the results.

Optical pyrometers, on the other hand, are used remotely, and are therefore nonperturbing. Since they measure some property of a radiating surface, they are also ideal for measurements at high temperatures, where the radiation intensity is high. The commonly used optical pyrometers are intensity pyrometers -- they compare the intensity of the surface radiation within a narrow wavelength range with the intensity of an adjustable internally heated source. This usual method of measurement is also very slow, however, and is not, in its conventional form, capable of following temperature changes of microsecond durations. Intensity pyrometry is also more subject to

inherent errors, such as window transmission and the deviation of the source of radiation from that of a black body than the method about to be described.

The method proposed here is two-color radiation pyrometry. Like conventional pyrometry, it is a remote sensing technique and therefore nonperturbing. Instead of measuring the intensity of the radiation of a surface at one wavelength, it utilizes the ratio of the intensities at two wavelengths, generally close to one another. Because the ratio is being measured rather than an absolute intensity, the method requires no correction for the transmission of the window providing the window has the same transmission at both wavelengths, a requirement that is usually easily met.

TWO-COLOR PYROMETRY

The measurement of temperature by optical pyrometry is based on the fact that for a black body, the power emitted at a given wavelength is determined by the temperature alone, and is given by the well known expression:

$$I_o(\lambda,T) = \frac{2hc^2}{\lambda^5} \frac{1}{\exp(hc/\lambda kT-1)} \qquad (5)$$

Where c is the velocity of light, λ is the wavelength, and h and k are Plank's and Boltzman's constants. For real surfaces, which are generally not black bodies, the emissivity, $\varepsilon(\lambda,T)$ must be taken into account, Equation (5) becomes

$$I(\lambda,T) = (\lambda,T)\ I_o\ (\lambda,T) \qquad (6)$$

Equation (6) forms the basis for intensity pyrometry. For accurate temperature measurements, corrections must be made for the emissivity of the surface. Consequently, there exist many tables of emissivity vs temperature and wavelength for various materials[17].

Two-color radiation pyrometry depends not on a determination of intensities, but on a measurement of the ratio of the relative radiation intensities at two different wavelengths. Let R be the ratio of the radiative intensities at λ_1 and λ_2. Then, since $\exp(hc/\lambda kT) > 1$,

$$R = \frac{I(\lambda_1)}{I(\lambda_2)} = \left(\frac{\varepsilon_1}{\varepsilon_2}\right) \left(\frac{\lambda_1}{\lambda_2}\right)^{-5} \exp\left(\frac{hc}{kT}\right) \left(\frac{1}{\lambda_2} - \frac{1}{\lambda_1}\right) \qquad (7)$$

It is worthwhile to compare intensity pyrometry with two-color pyrometry. For intensity pyrometry, a temperature accuracy as high as $\pm$ $5^{\circ}K$ can be obtained at $2000^{\circ}K$ with NBS calibrated reference sources. The dependence on an accurate knowledge of the emissivity is not great. For example, at $2000^{\circ}K$, and at 0.65 μm, a 10% error in the emissivity leads to a 0.65% error in temperature. An error analysis of the two methods indicates that the two-color method can be generally more accurate and more sensitive.[18] In particular, if ε_1 and ε_2 vary with temperature in the same way, errors in two-color pyrometry can be very small.

SENSITIVITY OF TWO-COLOR PYROMETRY

The sensitivity of two-color pyrometry (assuming constant emissivities) is given by

$$\frac{dR}{dT} = \left(\frac{\varepsilon_1}{\varepsilon_2}\right) \frac{hc}{kT^2} \left(\frac{1}{\lambda_2} - \frac{1}{\lambda_1}\right) \qquad (8)$$

dR/dT clearly depends on the choice of wavelengths. The closer the wavelengths are to one another, the lower the sensitivity. Two convenient wavelengths for which emissivity data is available are λ_1 = 0.665 μm and λ_2 = 0.463 μm.[2] Approximate values of ε_1 and ε_2 are shown in Figure 2. For these wavelengths,

$$R = 0.1636 \left(\frac{\varepsilon_1}{\varepsilon_2}\right) \exp\left(\frac{9.45 \times 10^3}{T}\right), \text{ and} \qquad (9)$$

$$\frac{dR}{dT} = \left(\frac{\epsilon_1}{\epsilon_2}\right) \frac{9.45 \times 10^3}{T^2} R \qquad (10)$$

Values for ϵ_1, ϵ_2, R, and dR/dT are given in Table 1 for temperatures of interest.

TABLE 1

T,K	ϵ_1	ϵ_2	R	dR/dT
3000	.388	.426	3.48	3.65×10^{-3}
2500	.399	.446	6.44	9.74×10^{-3}
2000	.414	.464	16.46	3.89×10^{-2}
1500	.432	.489	78.71	3.31×10^{-1}
1000	.452	.517	1818	17.2

Table 1 indicates that to cover the entire temperature range in a single measurement, a dynamic range of 1818/3.48 ≈ 500 is required of the detector without a change in sensitivity. With a detector accuracy of 1%, a 10 degree change at 3000K can be determined. This is quite a bit better than is needed. The dynamic range is a function of the wavelengths chosen and can be made smaller or greater by choosing wavelengths that are closer or further apart.

IMPLEMENTATION

To obtain the temperature profiles in the necessary times requires a detector with the following properties:

- o A speed of response of $< 10^{-6}$ sec;
- o A dynamic range of ~1000 or greater;
- o Adequate sensitivity;
- o Ability to obtain spacial information.

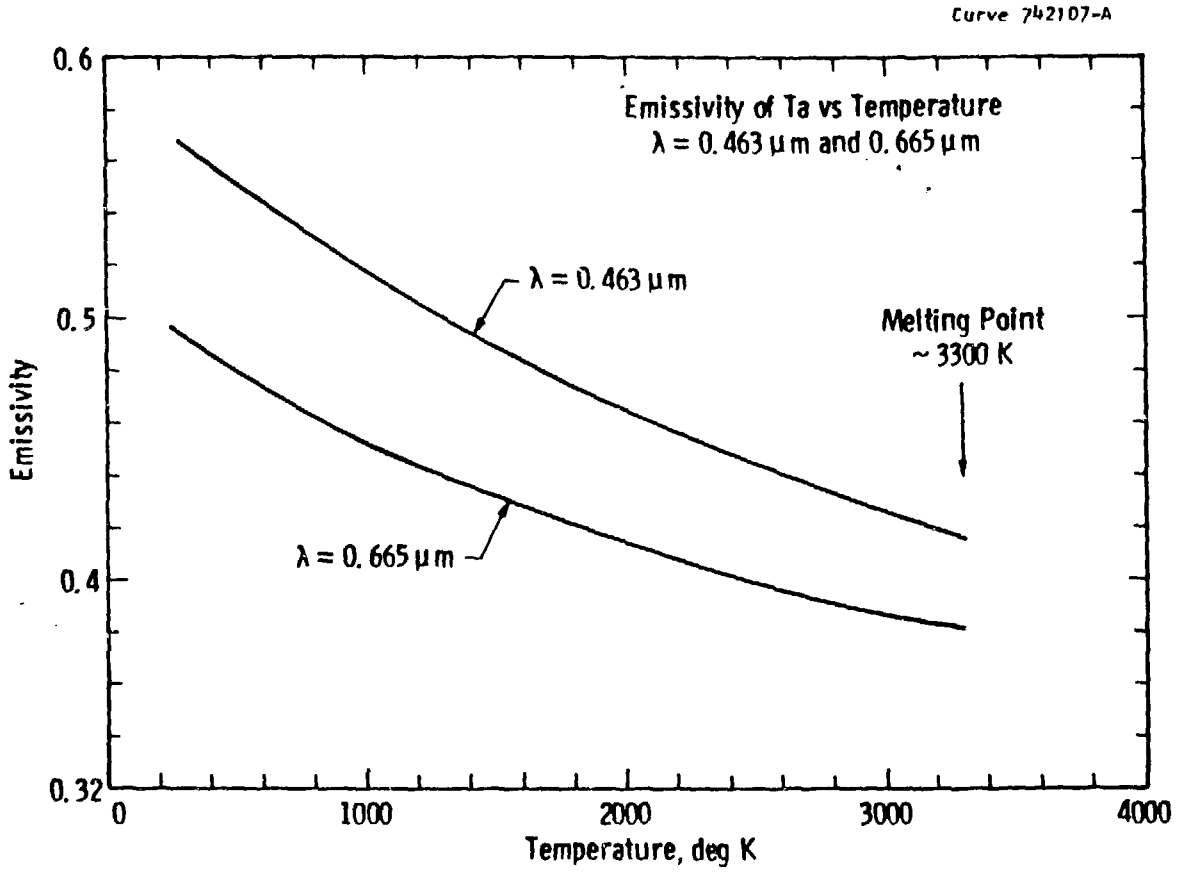

Fig. 2 - Emissivity vs. temperature for Ta.

Photomultipliers are generally capable of easily meeting the first three requirements. The fourth requirement is best met by using a vidicon detector. A proposed method of measurement utilizing a vidicon detector is shown in Figure 3.

Imagine a surface bombarded with a very short burst of energy simulating a pellet explosion. The temperature will instantaneously reach a very high value within the irradiation zone. At some later time, t, as heat diffuses both into and along the surface, the temperature of the surrounding area will have increased, while the irradiation zone temperature will have diminished. An image of this surface on an area-sensitive detector will produce a signal variation across the face of the detector that is proportional to the radiation emitted by the heated surface over the area being imaged. If the detector is gated so as to be active for a short time Δt and delayed by a time t after the time of the irradiation, the detector signal would correspond to an instantaneous measure of the profile of the surface temperature at time t after irradiation. By taking a series of these temperature "snapshots" with varying delay times, t, it is possible to obtain a series of profiles showing the time development of the diffusion of heat across the surface. By imaging the cross section of the irradiated plate, a similar set of profiles could be obtained for the diffusion of heat into the wall.

The above description does not yet provide the temperature information needed. To obtain the temperature, we split the initial image into two images. These are focussed one above the other on the face of a two section vidicon. Each image is identical except that each passes through a separate narrow band optical filter tuned to 0.665 μm and 0.463 μm respectively. The point by point ratio of the two filtered signals generated across the vidicon provides the information needed to calculate the temperature profile.

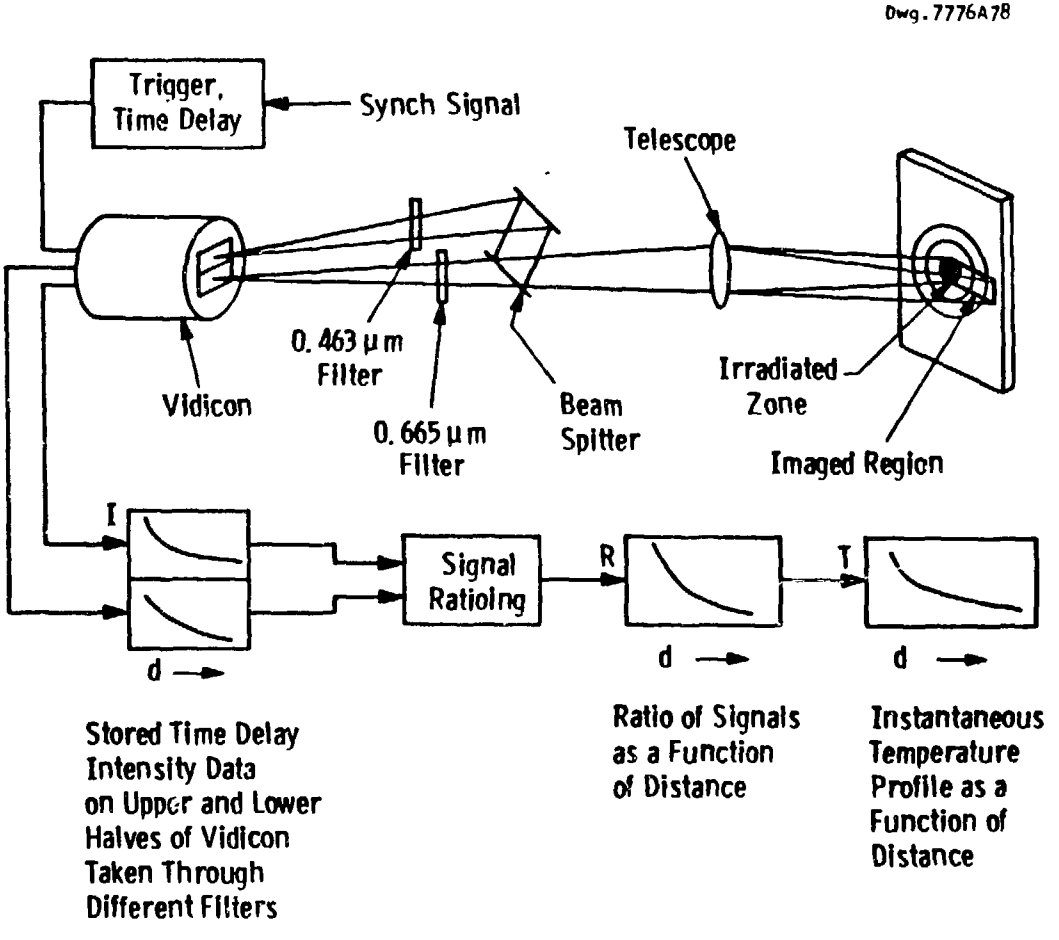

Fig. 3 - Schematic design for high-speed two-color optical pyrometry.

Vidicons that have the above requirements are commercially available. Listed below are the characteristics of an EGG model 1254 SIT vidicon detector:

Target Area:	12.5 mm high x 16 mm wide
Spectral Range:	0.350-0.800 μm
Dynamic Range:	1×10^4
Gating Speed:	4×10^{-8} sec, minimum
Number of Horizontal Channels:	256
Sensitivity:	2 photons/count
Uniformity of Sensitivity:	±10% over/cm area

The instrument used with the above vidicon, a PAR Optical Multichannel Analyzer, has within it the potential computer power to store the instantaneous images obtained, to obtain the ratios, and to perform the necessary calculations needed to generate the temperatures. Two such instruments with somewhat different characteristics exist in these laboratories. Thus, the basic capabilities for obtaining the temporal and spacial variation of the temperature following a simulated first wall irradiation can be obtained.

4.3 Measurement of Surface Deformation

GENERAL DISCUSSION

As mentioned in Section 2.2, a rapid intense heating of a localized region of a simulated first wall sample will bring about a deformation of the surface. This deformation will be related to the stresses created within the wall. Because the simulation will involve relatively small sample areas, the deformations produced by the heating are expected to be small, despite the very high temperature range involved. (For example, the linear expansion coefficient of Ta at 2000K

is ~7.4 x 10^{-6} m/mK). Thus, macroscopic measurements of displacement are not suitable. In addition, the requirements for remote, non-invasive measurement techniques applies equally well to these measurements as they do to temperature, thus eliminating such devices as strain gauges. The preferred method involves the use of optical techniques, and the conventional way of optically measuring small displacements is by interferometry. Conventional interferometry, such as Mach-Zehnder or Michelson, is very difficult to adapt to the present problem. A much more appropriate technique is that of holographic interferometry, and in particular, pulsed holographic interferometry. The latter is particularly suited to the present problem not only because it permits measurements on a scale of 2 x 10^{-8} sec, but also because it eliminates many of the problems encountered in cw holography.

HOLOGRAPHIC INTERFEROMETRY

A hologram is a recording, usually on a high resolution photographic plate, of the stationary interference pattern produced by the interference of light coming from a reference beam and that produced by the object in question, called the "scene" or "subject" beam. Because the hologram is itself an interference pattern, it is important to differentiate between the interference pattern that constitutes the hologram, a microscopic interference pattern, and the macroscopic pattern produced by the interferometer which measures the deformations induced in a surface.

To produce a hologram, one needs two coherent beams from a common source, one to serve as a reference beam, and the other to illuminate the object. Both beams originate from a common source. As shown in Figure 4, an expanded laser beam passes through a beam splitter. One portion of the beam is the reference beam, which falls directly on a high resolution photographic film. The remainder illuminates the subject, which in this case is the ICF wall surface.

Dwg.7776A79

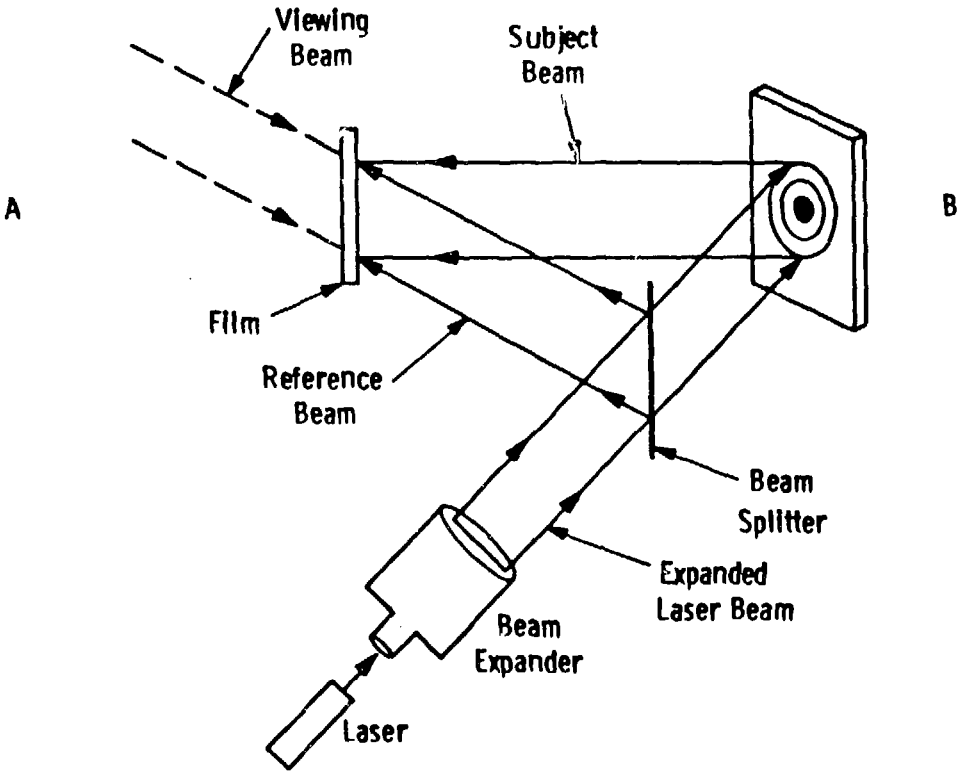

Fig. 4 - Schematic arrangement for producing holograms.

The light reflected from the subject falls also on the photographic plate, and constitutes the subject beam.

The microscopic stationary interference pattern recorded on the film constitutes the hologram. To view the hologram, the film is processed and examined with coherent illumination. A coherent source is allowed to illuminate the film along a direction identical to that taken by the original reference beam. An observer at A looking through the film will see a virtual image of the subject in a position identical to that occupied by the original subject. If on the other hand, the observer is at B and views the film by illumination in a direction opposite to that taken by the reference beam, as shown by the dotted lines, he will see a real image where the subject stood. Three dimensional images can be formed by diffusing the subject beam, for example by interspersing a diffuser plate between the beam splitter and the subject.

To form a holographic interferogram requires a double exposure taken on the same film. The first exposure is that of the subject in its normal unperturbed position. The second exposure is identical to the first, but with the subject in its deformed state. The photographic film then contains a record of two holograms, corresponding to the normal and to the deformed subject. When the hologram is processed and viewed as described above, one sees an image of the subject with superimposed light and dark interference fringes. These fringes correspond to phase differences between the two nearly identical images of the undeformed and deformed subject. As in normal interferometry, dark fringes appear at path length differences corresponding to integral multiples of $\lambda/2$. By counting fringes, displacements can be determined to a fraction of the wavelength. To form a permanent record, a normal photograph is taken of the holographic image.

Double exposure holographic interferometry has some very important advantages over normal interometr,. Among them are:

- o Since the interference pattern compares only the initial state of a surface with a displaced state, effects due to imperfect windows and other optical distortions cancel and need not prevent the interference pattern from forming. Normal interferometry requires the use of optically flat windows and surfaces.
- o For similar reasons, interference holograms of rough or curved surfaces can easily be obtained. Classical interferograms of such surfaces are very difficult or impossible to obtain.
- o As indicated earlier, three dimensional interferometry with large depth of field is possible with diffuse subject illumination. This has no counterpart in normal interferometry.
- o Much greater ease of alignment, a matter of great importance for complex experiments.

PULSED INTERFEROMETRY

For high speed phenomena, pulsed holographic interferometry is required. The basic arrangement is identical to that pictured in Figure 4, except that a pulsed laser is used as the coherent light source. There are, however, some practical differences, mostly advantageous. These derive from the fact that during the taking of a hologram the total optical path length must not vary by more than $\lambda/2$. C.w. holograms require considerable overall mechanical stability of the apparatus. Because the exposure times are of the order of 2×10^{-8} sec, pulsed holograms are virtually immune to vibration. As with c.w. holograms, it is important that between the initial hologram and that of the displaced subject, only the desired subject must be displaced or deformed; otherwise the holographic interferogram will record the total difference in path length due to all contributing motions. It is also

desirable that the illumination for the two exposures be nearly equal in order to produce fringes of maximum contrast.

IMPLEMENTATION

The best source is a Q-switched ruby laser. Pulse widths of ~2 x 10^{-8} sec are normally obtained. These speeds are more than adequate for the present diagnosis. Pulse-to-pulse stability of 10% is possible, and is adequate for good contrast. A coherence length of 5m is desirable and is available with single mode ruby laser oscillators or oscillator-amplifier combinations that are specifically designed for holographic use. High speed high resolution films have been developed in recent years, designed specifically for pulsed ruby laser holography. The literature is replete with examples of pulsed holographic measurements of high speed phenomena.[4,5] The application of pulsed holographic interferometry should in principle, therefore, present no serious problems in the present application. Indeed, the fact that the wall surfaces will be essentially specular makes the measurements relatively easy to perform.

As with the measurements of temperature, the deformation measurements would consist of obtaining interferograms of the surface at varying times, t, following the simulated pellet explosion. The sequence of events would be as follows:

1. The laser is pulsed, and an exposure is obtained of the unperturbed wall surface;
2. The simulated fusion explosion occurs;
3. At some variable time t following the explosion, the laser is pulsed again and a second exposure is obtained.

The interferogram obtained from 1 and 3 is a record of the deformation present at time t after the pellet explosion. By varying t, a complete history of the deformations can be obtained.

As with temperature measurements, it may be desirable to obtain interference patterns for the edge as well as the Ta surface. It may also be worthwhile observing the deformation of the rear surface of the wall to measure propagation through the wall.

4.4 Discussion of Diagnostic Techniques

Much of the success of the diagnostics described above will depend on the design of the overall simulation system. The presence of suitable windows, viewing angles, and adequate space for the measurements will be critical, and will need to be incorporated early in the design of the facility. A major uncertainty is the amount of electrical and radiation shielding that will be necessary. Because both sets of proposed measurements are optical, some immunity from radiation can be gained by choosing longer measuring distances. In the case of the proposed temperature measurements, a critical element is a suitable imaging system for the two-color pyrometry. The use of a vidicon for this purpose is novel. Fortunately, alternative methods are possible for performing high speed two-color pyrometry (for example, with conventional photomultiplier tubes) so that the measurements are not wholly dependent on the exact method described here. Since all of the proposed measurements are sequential in nature, that is to say, measurements are to be taken at varying times, t, after the simulated explosion, it is important to maintain a high degree of stability and reproducibility in the simulated explosions from pulse to pulse. A variation of $\pm 10\%$ is probably adequate. Larger variations may require some sort of averaging of events, which can increase the time required to obtain good results. Finally, while it would be desirable to measure the temperature and surface deformation simultaneously, such simultaneous measurements are likely to present many complications. It will generally be sufficient to obtain the two measurements independently, and to correlate them later. Through such correlations, it should be possible to theoretically deduce the stresses induced in the ICF first wall in actual fusion experiments.[23,24]

5. ACKNOWLEDGEMENTS

The authors wish to thank the Westinghouse Advanced Energy Systems Division, and Dr. E. W. Sucov, Manager, Fusion Projects, for their generous support of this project. In addition, we acknowledge the wholehearted support of the Office of Inertial Fusion, DOE, and the national laboratories in guiding this effort and supplying information and advice. Special appreciation is expressed to I. Bohachevsky, LANL; T. Godlove, OIF, DOE; M. J. Monsler, LLNL; and to our contract monitor, Rex. B. Purcell.

This work was performed under U.S. Department of Energy Contract DE-AC-08-81DP40146.

6. REFERENCES

1. T. Kammash, Fusion Reactor Physics Principles and Technology, Ann Arbor Science Publishers, Ann Arbor, MI, (1975).

2. L. D. Landau and E. M. Lifshitz, Fluid Mechanics, Addison-Wesley Publishing Co., Reading, MA (1959).

3. R. R. Peterson and G. A. Moses, "Blast Wave Calculations in Argon Cavity Gas for Light Ion Beam Fusion Reactors," UWFDM-315 (1979).

4. M. A. Sweeney and D. L. Cook, "Blast-Wave Kinetics and Thermal Transport in a Particle-Beam Reactor Chamber," Sandia Laboratories Preprint (1980).

5. C. J. Sparks, Jr., "Research with X-Rays," Phys. Today 34, 40 (1981).

6. W. B. Westerveld, A. McPherson, and J. S. Risley," Synchrotron Radiation Intensity for 50-MeV to 50-GeV Electrons," At. Data & Nuc. Data Tables 28, 21 (1983).

7. A. Barrie, "Instrumentation for Electron Spectroscopy," Chapter 2, Handbook of X-Ray and Ultraviolet Photoelectron Spectroscopy, D. Briggs, ed., Heyden, Philadelphia, PA (1978).

8. R. H. Hughes, T. A. Heumier, and P. M. Griffin, "Vacuum UV and Soft X-Ray Optical Emissions from Electron Impact on Metals," Appl. Opt. 20, 1350 (1981).

9. T. Sagawa, "Soft X-Ray Emission and Absorption Spectra of Light Metals, Alloys, and Alkali Halides," 29, Soft X-Ray Band Spectra, D. J. Fabian, ed., Academic Press, New York, NY (1968).

10. A. N. Chu, M. A. Piestrup, T. W. Barbee, Jr., and R. H. Pantell, "Transition Radiation as a Source of X-Rays," J. Appl. Phys. 51, 1290 (1980).

11. Z. Yu, J. Rocca, J. Meyer, and G. Collins, "Transverse Electron Guns for Plasma Excitation," J. Appl. Phys. 53, 4704 (1982).

12. J. Hecht, "Laser Application Matrix," Lasers & Appl. (1982).

13. J. A. McKay, "Pulsed CO_2 Lasers for the Surface Heating and Melting of Metals," IEEE J. Quant. Electron. QE-17, 2008 (1981).

14. S. J. Thomas, R. F. Harrison, and J. F. Figueira, "Observations of the Morphology of Laser-Induced Damage in Copper Mirrors," Appl. Phys. Lett. 40, 200 (1982).

15. R. G. Wilson and G. R. Bremer, Ion Beams with Applications to Ion Implantation, Robert E. Krieger Publishing Co., Huntington, NY (1979).

16. L. H. Taylor and E. W. Sucov, "Coating Requirements for an ICF Dry Wall Design," J. Nuclear Materials 103, 245-250 (1982).

17. Thermophysical Properties of Matter, Y. S. Touloukian and D. P. DeWitt, editors, IFI/Plenum, New York, NY, (1970) Vol. 7, pp. 654-677.

18. E. C. Pjatt, "Some Consideration of the Errors of Brightness and Two-Color Types of Spectral Radiation Pyrometry," British J. Appl. Phys. 5, 264 (1954).

19. R. J. Collier, C. B. Burckhardt and L. H. Lin, Optical Holography, Academic Press, New York, NY (1971), Chapters 11 and 15.

20. I. O. Heflinger, R. F. Wuerker and R. E. Brooks, "Holographic Interferometry," J. Appl. Phys. 37, 642 (1966).

21. M. K. Bhattacharyya and D. T. Tuma, "Heating of Solid Targets by Electron Beams," IEEE Trans. Elect. Dev. (to be published).

22. T. G. Frank and C. E. Rossi, "Technology Requirements for Commercial Applications of Inertial Confinement Fusion," Nucl. Tech./Fus. 1, 359 (1981).

23. L. H. Taylor and G. B. Brandt, "An Error Analysis of Holographic Strains Determined by Cubic Splines," Exp. Mech. 12, 543 (1972).

24. G. B. Brandt and L. H. Taylor, "Holographic Strain Analysis Using Spline Functions," Proc. Eng. Appl. Holography Symposium, 123 (1972).